Design of new Cu-Fe metallic oxide foams formed by electrodeposition for asymmetric supercapacitors electrodes

Grzegorz Adam Lange

Extended abstract

1. Introduction

Increasing energy needs of modern societies is a phenomenon we are witnessing nowadays. There is a strong pressure on finding new alternative and innovative energy storage systems which can replace or complement conventional technologies which, in many cases, are insufficient in terms of capability and ecological concerns. This calls for shifting gears to new materials having improved properties.

Supercapacitors are considered the most promising candidate as energy storage devices since they comprise high power density, long cycling life as well as short charge/discharge time. These advantages make supercapacitors promising for use in automotive industry, space and aeronautical industry or mobile devices [1]. The performance of a supercapacitor is defined by the material that is used as electrode. Therefore, the development of new electrodes is one of the most challenging areas towards the development of advanced supercapacitors. In this field, transition metal oxides are becoming very attractive materials because of their pseudocapacitive electrochemical behavior [2]. Extensive studies are carried out on RuO_2 oxide since this crystalline or amorphous hydrous compound has high specific capacitance close to 700 Fg^{-1}. However, RuO_2 presents high toxicity and very high cost [3]. Other metal oxide which has drawn attention is MnO_2, which demonstrates several oxidation states that create pseudocapacitive character. Studies have shown, that thin MnO_2 films exhibit specific capacitances of approximately 700 Fg^{-1} [4]. The biggest disadvantage of manganese oxide in case of application for supercapacitors electrodes is its poor longtime-cycle performance. An alternative to MnO_2 is provided by Ni and Co oxides. It was reported that heat treated Co_3O_4 was able to reach 291 Fg^{-1} whereas $Co(OH)_2$ used as single electrode approached 280 Fg^{-1} [3]. In case of Ni oxides and hydroxides, obtained capacitances range from 278 Fg-1 (NiO), 578 Fg^{-1} demonstrated by $Ni(OH)_2$ and 1700 Fg^{-1} shown by combining Ni oxides with carbon nanotubes [3, 5].

Among the transition metallic oxides, Fe oxide is a very promising candidate for supercapacitors mainly due to its low cost and environmental friendliness. Generally, Fe_3O_4 electrodes do not manifest such high specific capacitances as it happens for MnO_2 or RuO_2. Literature gives values of specific capacitance of 5 – 7 Fg^{-1}, whereas this value can be increased up to 100 Fg^{-1} by optimization of the porosity and crystallinity of deposited Fe_3O_4 structures [6]. Studies on combining Fe_3O_4 with carbon black have allowed to obtain the highest specific capacitance value: 510 Fg^{-1} [7]. Intensive studies were also carried out on $Fe(OH)_3$ and FeO(OH) resulting in specific capacitance values of approximately 400 Fg^{-1} [8]. The need of cheap transition metals has also brought attention to Cu oxides. Studies on copper oxide films revealed that specific capacitances may vary between

6 Fg^{-1} to 43 Fg^{-1} [9, 10]. In order to improve these values it is possible to combine copper with other metals such as Fe or Ni to obtain alloys presenting higher capacitances.

Properly selected metal oxides, when deposited, can demonstrate high porosities as well as wide pore distribution which are sought characteristics in case of application as supercapacitors electrodes. These rough structures are called nanoporous metallic foams (NMFs) and are usually 3D structures of pores and interconnected nano-ramified walls.

In order to fabricate highly porous structures electrodeposition becomes very flexible, cheap and versatile method. By applying the right potentials (or currents), a dynamic template can be obtained. Thus, for the production on NMFs by electrodeposition, the dynamic template is formed by hydrogen bubbling, which is a spontaneous process that occurs simultaneously with metal deposition at the substrate. The process is very fast and highly dynamic hydrogen bubbling facilitates fast fabrication of metallic foams. This process is considered as a low-cost method. Moreover, by electrodeposition, the NMFs can be easily formed on metallic substrates having high electronic conductivity which is an advantage in the case of supercapacitor electrodes (direct application of active material on the current collector) [11].

The aim of this research was to develop and to test new electrodes based on NMFs of Fe and Cu for application as redox supercapacitor electrodes. By combining properties characteristic of metals (good electrical and thermal conductivity) with a high surface area and ultralow density it is possible to obtain a promising electrode material for high performance supercapacitor.

2. Material and solution

2.1. Substrate preparation and solution used

Electrodeposition was carried on the AISI 304 stainless steel plates (current collectors) with mass approximately 3.3 g. The chemical composition of the substrates is presented in Tab. 1.

Tab. 1. Chemical composition of AISI 304 stainless steel

Elements (%m/m)							
Cr	Ni	C	Mn	Si	P	S	Fe
18.0	10.0	0.08	2.0	1.0	0.045	0.03	68.845

First, the stainless steel plates were polished with SiC paper with 500, 800 and 1000 grit. After polishing, the substrates were cleaned in ultrasonic cleaner in acetone solution, rinsed with distilled water and dried with compressed air. Once the substrates were dried, they were weighted. After electrodeposition, substrates with deposited NMFs were rinsed gently with distilled water, dried with compressed air (at room temperature) and weighted.

The solution used for electrodeposition was prepared from analytical grade chemicals and distilled water. The final solution used consisted of 0.5 M $(NH_4)_2Fe(SO4)_2 \cdot 6H_2O$, 1.5 M H_2SO_4 and 0.01 M $CuSO_4$.

2.2. Electrodeposition set-up and parameters

Electrodeposition of nanostructured metallic foams (NMFs) was performed on AISI 304 stainless steel substrates using a 2-electrode electrochemical cell connected to a DC power source. The setup used for electrodeposition consisted of the following elements: *a)* stainless steel plate of dimensions of 2.0 x 2.5 cm (working electrode); *b)* cylindrical electrochemical cell (7.0 cm of height and 5.0 cm width) with lateral round hole of active area of 1.65 cm^2; *c)* platinum counter electrode. Electrodeposition parameters are presented in Tab. 2.

Tab. 2. Electrodeposition parameters

Applied time [s]	Applied current [A]	Current density [A/cm^2]
30, 90, 120, 180	0.825	0.5
30, 90, 120, 180	1.65	1.0
30, 90, 120, 180	2.475	1.5
30, 90, 120, 180	3.0	1.8

2.3. Thermal conditioning

Heat treatment at various temperature was implemented in order to examine the role of temperature in the chemical and physical properties of the deposited foams. Thus, the selected samples were subjected to thermal conditioning at 150 °C or 250 °C in a Memmert oven. The residential time was set on 2 hours in the case of each temperature.

3. Characterization techniques

3.1. Scanning electron microscopy (SEM)

Scanning electron micrographs were obtained with Hitachi S-2400 microscope using typically an acceleration voltage of 20 kV. This microscope provides an image resolution of 10 nm.

3.2. Energy dispersive X-ray spectroscopy (EDS)

EDS analysis was performed using a Rontec standard EDS detector attached to the Hitachi S-2400 SEM. EDS spectra analysis was performed by Wintools, comparing peak positions with a database for elemental identification.

3.3. X-ray diffraction (XRD)

X-ray diffraction was performed using a Bruker D8 Advance diffractometer with a Bragg-Brentano geometry working with Cu radiation (0.154056 nm). Phase identification is performed by the Hanawalt method, comparing the position of the three most intense peaks in the pattern with known patterns of pure substances referred in the ICDD database.

3.4. Electrochemical techniques – cyclic voltammetry (CV) and chronopotentiometry

Cyclic voltammetry studies were performed using a 3-electrode electrochemical cell connected to a Voltalab PGZ 100 potentiostat. The working electrode was the metallic deposited on a stainless steel substrate with an active area of 1 cm^2. The counter electrode was a platinum spiral electrode while saturated calomel electrode (SCE) played a role of reference electrode. All measurements were carried out in 1 M NaOH electrolyte at room temperature in potential window ranging from -1500 mV to 0 mV. The potential range selected for the experiments purposes satisfied the working potentials of pseudocapacitive-type materials basing on iron and copper [12].

Chronopotentiometry experiments were carried out in 1 M NaOH electrolyte at room temperature using the electrochemical set-up described for cyclic voltammetry. Applied current densities were 1 mA/cm^2 (charge) and -1 mA/cm^2 (discharge) in potential window ranging from -1000 mV to 200 mV. Chronopotentiometry technique was used to calculate specific capacitances of deposited foams as well as to carry out longtime performance test where sample was subjected to 8000 cycles of charge and discharge to identify its capacitance retention.

4. Results and discussion

4.1. Selection of samples

Three raw samples having the highest amount of Fe (on the basis of EDS analysis) were chosen for full characterization (Tab. 3.). Selected samples were subjected to heat treatment at

temperatures of 150 and 250 °C in order to determine if their performance was improved. Heat treated samples along with corresponding indices are presented in Tab. 4.

Tab. 3. Identification of raw samples selected for tests

	Deposition time [s]	Current [A]	Index
1.	90	2.475	90s_2.475A
2.	90	3.0	90s_3A
3.	180	3.0	180s_3A

Tab. 4. Description of heat treated samples

Raw sample index	Temperature [°C]	Index of heat treated sample
90s_2.475A	150	90s_2.475A_150C
	250	90s_2.475A_250C
90s_3A	150	90s_3A_150C
	250	90s_3A_250C
180s_3A	150	180s_3A_150C
	250	180s_3A_250C

4.2. Scanning electron microscopy (SEM)

Selected samples were analyzed by SEM in order to characterize the deposited structures. As can be noticed from the images below (Fig. 1 to 3), increasing time of deposition as well as applied current can significantly change the 3D foams. As it may be seen, dispersed dendrite structures have been formed over a continuous thin film composed of angular grains. Furthermore, spacing between the dendritic structures is approximately 20 μm (see squares in Fig. 1c), and may be related to the formation of hydrogen bubbles during deposition.

In the films deposited at a higher current (3 A) for 90 s (Fig. 2), the density of dendritic structures formed increases and a network of dendritic walls is formed. The dendrites do not present any preferential growth direction (in relation to the substrate), being randomly oriented. As indicated in Fig. 2c (white squares), the distances between the dendritic structures are slightly smaller than in sample 90s_2.475A, ranging from 15 to 20 μm.

Films prepared at 3 A for 180 s are shown in Fig. 3. The continuous thin film formed at the substrate's interface is still visible, but, and contrarily to the previous samples, a 3D honeycomb-like dendritic structure is also observed, similarly to other studies on copper electrodeposition. The formation of this structure is related to hydrogen bubbles forming at the active sites during the electrodeposition process. Due to the high cathodic current applied, deposition of Cu and Fe occurs simultaneously with intense hydrogen evolution, which is easily seen during deposition experiments. Metal deposition occurs preferentially in the space between hydrogen bubbles, forming metal grains. H_2 bubbles grow (or coalesce) with time and eventually detach from the substrate, creating regular shaped pores in the growing deposit. Furthermore, hydrogen bubbles will also evolve at different locations and depths in the growing metallic foam, leading to a wide size distribution of surface pores.

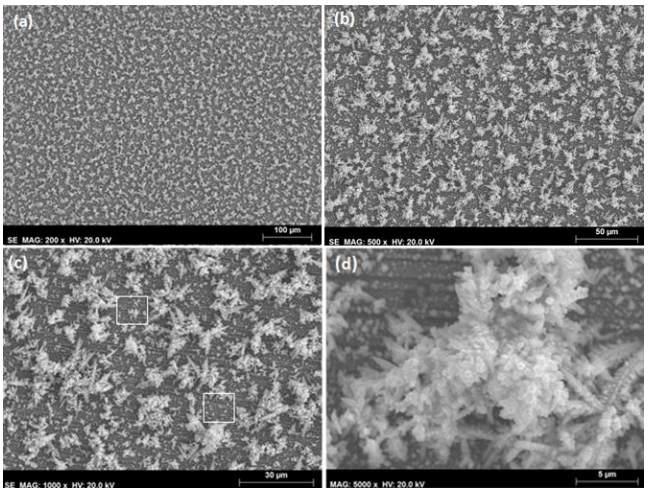

Fig. 1. SEM images of Cu-Fe deposits for sample 90s_2.475A at different magnifications: a) 200x, b) 500x, c) 1000x, d) 5000x.

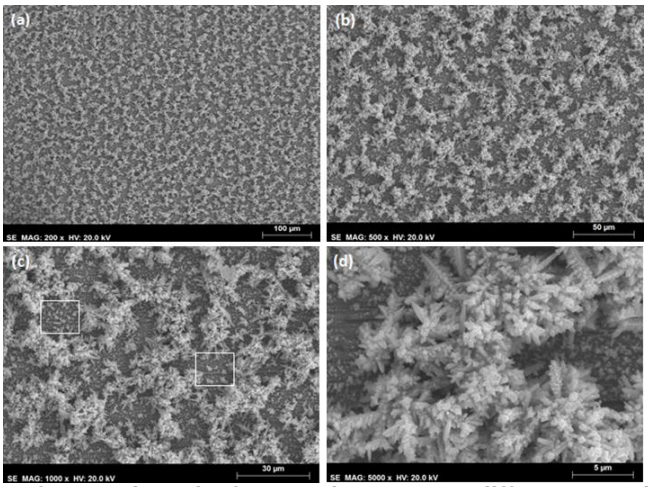

Fig. 2. SEM images of Cu-Fe deposits for sample 90s_3A at different magnifications: a) 200x, b) 500x, c) 1000x, d) 5000x.

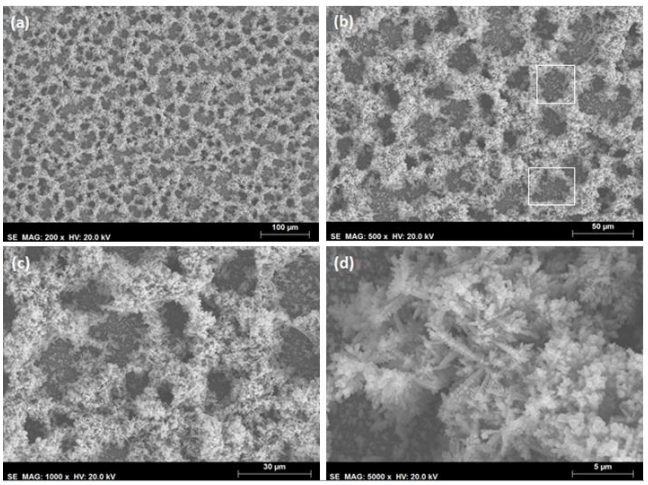

Fig. 3. SEM images of Cu-Fe deposits for sample 180s_3A at different magnifications: a) 200x, b) 500x, c) 1000x, d) 5000x.

As can be seen in Fig. 3, there are different types of holes/craters in the deposits, marked with white squares in Fig. 3b. One type (upper square) presents a nearly circular shape and originates from the formation of hydrogen bubbles at the substrate around which the metal will deposit. A second type of craters (lower square) presents an irregular shape and their formation may be explained by the

nucleation and growth of adjacent metal grains that will join the closely formed agglomerates and thus form irregular holes [13].

SEM image of sample 90s_2.475A after heat treatment in 150 and 250 °C is presented in Fig. 4. As can be seen, images at magnification of 1000x do not differ in a significant way. The lengths of the spots covered with Cu-Fe grains remain the same comparing to the raw sample. The structure was not broken and remains nearly unaltered after heat treatment. However, higher magnification images (5000x) show that the grain size of the deposited film increases with the heat treatment temperature (white squares in Fig. 4d and 4f). This result is attributed to the oxidation process.

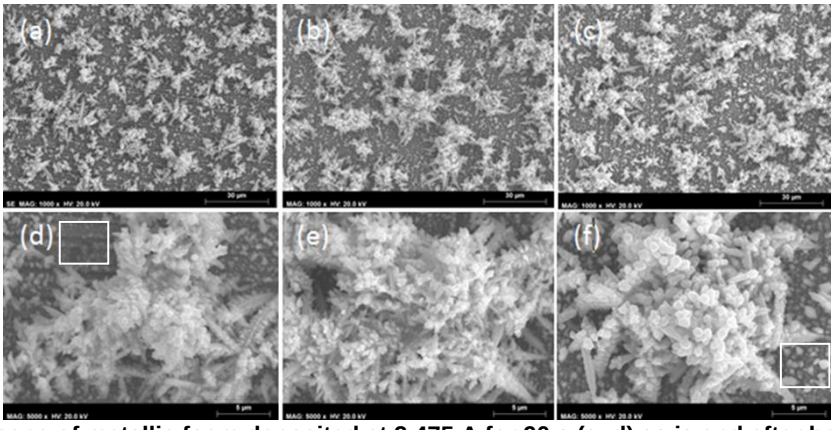

Fig. 4. SEM images of metallic foam deposited at 2.475 A for 90 s (a, d) as is and after heat treatment at (b, e) 150 °C and (c, f) 250 °C.

High magnification images show that the branches of the dendrites become coarser after heat treatment and this phenomenon occur in each sample.

4.3. Energy dispersive X-ray spectroscopy (EDS)

Chemical composition of the electrodeposited foams was studied by EDS and, as expected, the main elements detected were copper and iron. A typical EDS spectrum of the metallic foam obtained at 2.475 A for 90 s is presented in Fig. 5.

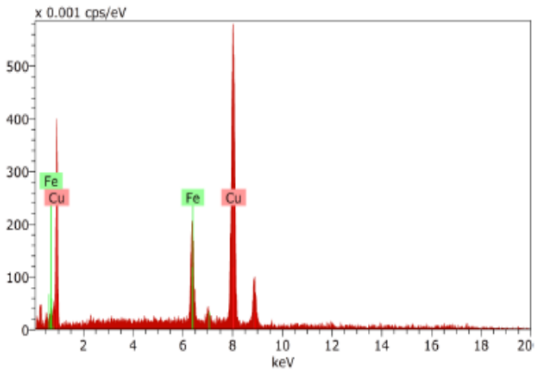

Fig. 5. EDS spectrum of metallic foam obtained at 2.475 A for 90 s.

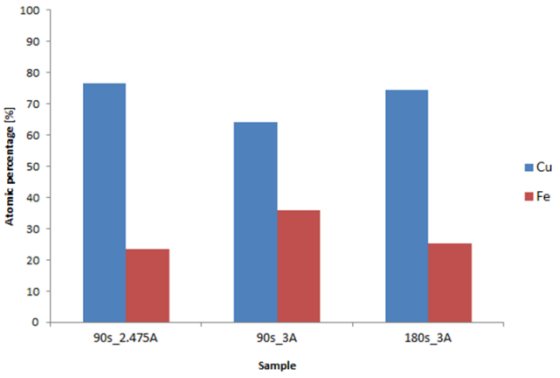

Fig. 6. Variation of Cu and Fe content of the foams with the deposition parameters.

Dependence of the average Cu and Fe atomic percentages in the films on the deposition conditions is shown in Fig. 6. Iron content of the metallic foams tends to increase with the applied current density and decreases with deposition time. Increased current of electrodeposition process resulted in increasing Fe content in samples obtained after 90 seconds (from 23 % to 36 %). In the case of sample 180s_3A, improved time resulted in identical proportions of metals as found in sample 90s_2.475A. It means that in order to obtain more iron in the foam structure it is necessary to limit the deposition time due to more intense copper deposition after a period of 90 seconds.

It should also be noted that the copper content in the foams is much higher than that in the deposition electrolyte. In solution, copper represents only 2 at. % of the metallic ions but it reaches up to almost 80 at. % in metallic foams. The standard reduction potential of copper (+0.337 V) is about 0.7 V less negative (more noble) than that of iron (-0.41 V). Hence, during electrodeposition of Cu-Fe foams, Cu, being the most noble metal, deposits preferentially to Fe, explaining the reason why the content of Cu in the deposited foam is higher than in solution.

EDS analysis was also performed in the same three samples after heat treatment (at 150 and 250 °C). As expected, the only difference is that heat-treated samples present oxygen in their chemical composition with atomic percentage ranges from approximately 10 % (at 150 ºC) up to 28 % (at 250 ºC).

4.4. Dependency of deposited mass on current density and deposition time.

As expected, the mass of deposits increases with the deposition time and the applied current. This behavior is presented in Fig. 7. In order to present increasing character, the additional samples are included i.e. 0.825 A and 1.65 A for 90s as well as 0.825 A, 1.65 A and 2.475 A for 180s. The obtained results for deposit mass indicate that current which is applied plays significant role in electrodeposition process in this study. The time which is used is also a factor that improves the mass of deposited foams.

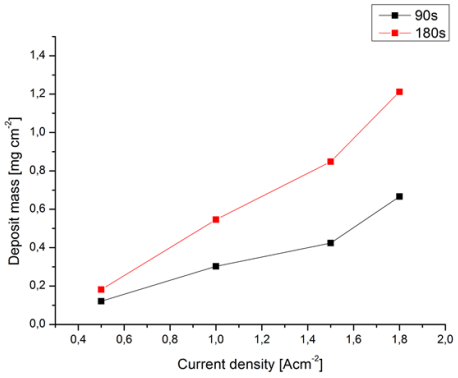

Fig. 7. Relationship between deposit mass and applied current density.

4.5. XRD analysis

XRD analysis was carried out on Cu-Fe foams deposited at 3A for 180 s before (sample 180s_3A) and after heat treatment at 150 ºC (180s_3A_150C) and 250 ºC (180s_3A_250C). The resulting diffractograms are presented in Fig. 8. The diffractogram of sample 180s_3A contains four peaks. The peaks at 43.4°, 50.5° and 74.2° correspond to (111), (200) and (220) planes of face-centered cubic copper (ICDD 01-070-3039), respectively. Peaks related to an iron phase were identified at 44.6° and 82.3° which are attributed to (110) and (211) planes of body-centered cubic iron (ICDD 03-065-4899). This result is also in agreement with other studies in the literature [14].

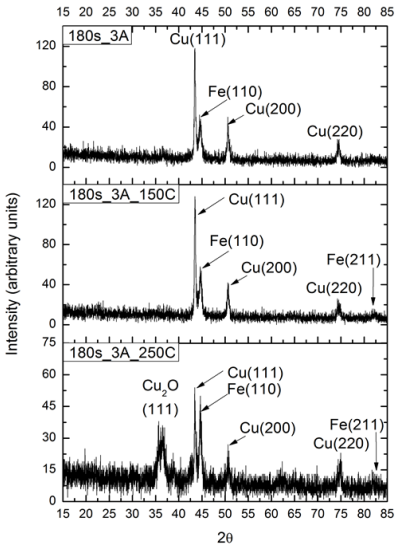

Fig. 8. Diffractograms of Cu-Fe foams obtained at 3A current and 180s before and after heat treatment.

After heat treatment at 150 °C, the diffractogram does not present significant changes (Fig. 8). After heat treatment at 250 °C a new peak is observed at 36.4º which corresponds to (111) plane of Cu_2O (ICDD 077-0199). These results indicate that the heat treatments lead to the partial oxidation of the Cu-Fe films and to the formation of Cu_2O, in agreement with the EDS results that indicated a high oxygen content. Peaks related to the formation of iron oxides could not be identified at the diffractograms, probably due to the small amount of that phase.

4.6. Cyclic voltammetry

Representative cyclic voltammograms of Cu-Fe foams (Figs. 9 and 10) are not square-shaped as those of materials that exhibit an electric double layer charge storage mechanism [15]. Electrochemical behavior of the tested samples is very similar.

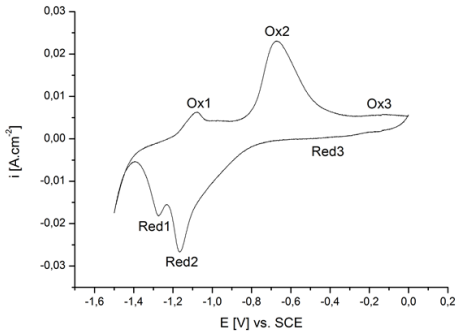

Fig. 9. Typical peaks occurring in the voltammograms. Sample 90s_2.475A_150C. Scan rate 50 mV/s.

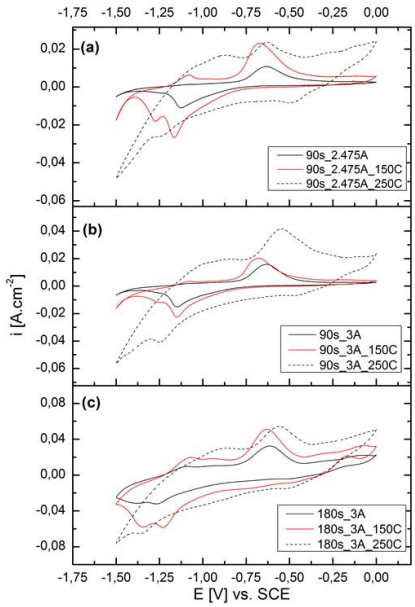

Fig. 10. Cyclic voltammograms of Cu-Fe foams before and after heat treatment in 1 M NaOH. Scan rate 50 mV/s.

In general, three reduction peaks and three corresponding oxidation peaks can be identified (Fig. 9) and related to the following reactions [16, 17, 18]:

Ox1/Red1: $Fe + 2OH^- \leftrightarrow Fe(OH)_2 + 2e^-$

Ox2/Red2: $2Cu + 2OH^- \leftrightarrow Cu_2O + H_2O + 2e^-$

Ox3/Red3: $Cu_2O + 2OH^- + H_2O \leftrightarrow 2Cu(OH)_2 + 2e^-$

Fig. 10 depicts cyclic voltammograms from all raw samples and their heat treated correspondents. Cyclic voltammograms of heat treated samples show larger redox peaks. This is attributed to the enhancement of these redox reactions due to the oxidation of the foams during the heat treatment.

4.7. Chronopotentiometry tests

Fig. 11 presents the second charge/discharge curves of the raw 90s_2.475A and corresponding heat treated samples. Basing on Eq. 1 and time of discharge (from 0.2 V to -1.0 V), specific capacitance was calculated.

$$C = \frac{i\Delta t}{m\Delta V} \qquad \text{Eq.1.}$$

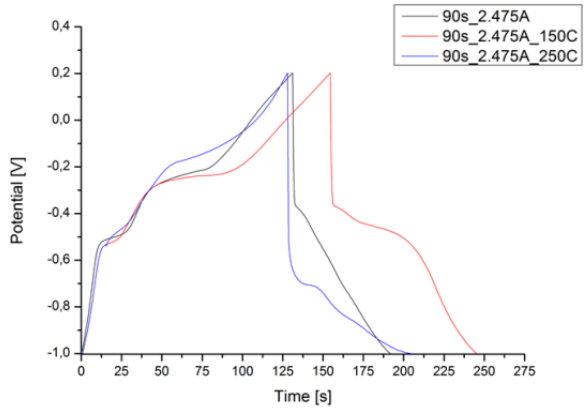

Fig. 11. Comparison of charge-discharge curves of raw and heat treated samples obtained in 90s and 2.475A current.

Raw sample demonstrates specific capacitance of 137 Fg^{-1} while sample treated at 150 °C exhibits the best performance in terms of time of charge-discharge and related specific capacitance (205 Fg^{-1}). Sample after heat treatment at 250 °C resulted in obtaining 176 Fg^{-1}.

Raw sample 90s_2.475A was also subjected to longtime cycle performance in potential window -0.9 V to -0.2 V. Resulting plot is presented in Fig. 12.

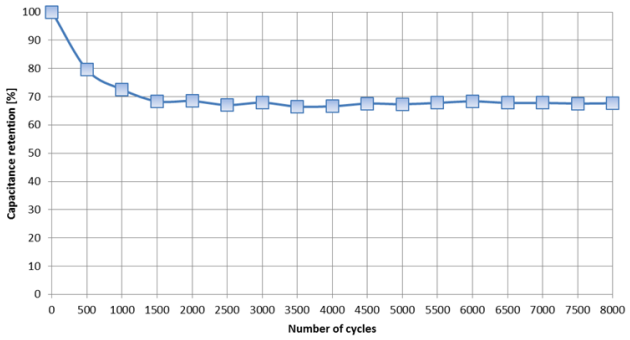

Fig. 12. Capacitance dependency on number of cycles (vs. SCE).

The specific capacitance decreased by approximately 33.5 % until the 2500 cycle, stabilizing after that. From this moment the capacitance values stay more or less at the same level. The values obtained in this test show stability of the produced foams, which is a very important requirement for being used as electrodes for supercapacitors along with the number of charge-discharge cycles

5. Conclusions

The objective of the present work was to develop and test nanostructured metallic Cu-Fe foams for application as Cu-Fe as electrodes for supercapacitors. Metallic foams of Cu-Fe were produced by electrodeposition directly on stainless steel substrates that acted as the current collector.

The optimization of the electrodeposition parameters such as time and current resulted in selection of three raw samples: 90s_2.475A, 90s_3A and 180s_3A.

The morphological characterization of the deposited Cu-Fe foams proved, that increasing time of deposition as well as applied current can significantly change 3D foams. Due to high cathodic current, deposition of Cu and Fe occurs simultaneously with intense hydrogen evolution and thus characteristic craters are created.

Morphological characterization of samples subjected to heat treatment showed, that the structure was not damaged by treatment at 150 °C or 250 °C. It was noticed, that branches of dendrites of samples treated at 250 °C are coarser than the those in the structure of raw sample or treated at 150 ºC.

The EDS analysis revealed a dependence of Cu and Fe content on the deposition parameters. Samples 90s_2.475A, 90s_3A and 180s_3A show iron contents equal 23 %, 36 % and 25 %, respectively. It means, that in order to obtain more iron in the foam structure it is crucial to limit time of deposition due to more intensified copper deposition after a period of 90 seconds. Tests on heat treated samples have shown that oxygen content has increased from 10 % (at 150 °C) to 28 % (at 250 °C).

XRD analysis provided information about planes of face-centered cubic copper and body-centered cubic iron. Diffraction patterns of sample subjected to heat treatment at 150 ºC do not differ from the diffraction patterns of raw samples. In the case of the sample treated at 250 ºC, new peak raised and corresponds to Cu_2O. The resulting diffractograms show that heat treatments lead to the partial oxidation of Cu-Fe films. Peaks related to iron oxides could not be identified, probably due to the small amount of that phase.

Cyclic voltammetry carried out in the potential window of -1.5 V to 0 V in 1 M NaOH revealed three reduction peaks and three corresponding oxidation peaks. This phenomenon is related to pseudocapacitive behavior of the deposited foams. Moreover, existing peaks correspond to Fe and Cu redox reactions what leads to a conclusion, that co-deposition of these metals occurred. Results also showed, that the higher current, the bigger the specific area of the voltammogram. Increased specific area and intensified peaks can also be observed in the case of heat treated samples. The explanation is that heat treatment resulted in oxidation of foams present on the substrates and thus redox reactions are intensified.

The chronopotentiometric tests revealed that sample 90s_2.475A, and its heat treated correspondents, provided the best results in terms of stability. The highest specific capacitance was obtained for the 90s_2.475A_150C sample and was equal 205 Fg^{-1}. During longtime-cycle performance 8000 cycles of charge-discharge were carried out on the sample 90s_2.475A. The specific capacitance decreased by nearly 33.5 % until the 2500 cycle, stabilizing after that. The values obtained in this test showed good stability of the produced Cu-Fe foams.

Tests on Cu-Fe foams resulted in specific capacitance of 205 Fg^{-1}. This value is higher than results from other studies on Cu oxides (up to 43 Fg^{-1}) and Fe oxides (up to 100 Fg^{-1}) mentioned in the beginning.

References

[1] Qu Q., Yang S., Feng X. (2011), *2-D sandwich-like sheets of iron oxide grown on graphene as high energy anode material for supercapacitors*, Advanced materials, Volume 23: 5574-5580

[2] Zhang Y., Feng H., Wu X., Wang L., Zhang A., Xia T., Dong X., Li X., Zhang L. (2009), *Progress of electrochemical capacitor electrode materials: A review*, International Journal of Hydrogen Energy 34, 4889-4899

[3] Lokhande C.D., Dubal D.P., Joo O-S. (2011), *Metal oxide thin film based supercapacitors: A review*, Current Applied Physics 11, 255-270

[4] Wei J., Nagarajan N., Zhitomirsky I. (2007), *Manganese oxide films for electrochemical supercapacitors*, Journal of Materials Processing Technology 186, 356–361

[5] Zhao D., Bao S., Zhou W., Li H. (2007), *Preparation of hexagonal nanoporous nickel hydroxide film and its applications for electrochemical capacitor*, Electrochemistry Communications 9, 869-874

[6] Nagarajan N., Zhitomirsky I. (2006), *Cathodic electrosynthesis of iron oxide films for electrochemical supercapacitors*, Journal of Applied Electrochemistry 36:1399-1405

[7] Wang S-Y., Ho K-C., Kuo S-L., Wu N-L. (2006), *Investigation on Capacitance Mechanisms of Fe3O4 Electrochemical Capacitors*, Journal of The Electrochemical Society 153 (1) A75-A80

[8] Hallam P.M., Mingot M.G., Kampouris D.K., Banks C.E. (2012), *Facile synthetic fabrication of iron oxide particles and novel hydrogen superoxide supercapacitors*, RSC Advances 2, 6672-6679

[9] Patake V.D., Joshi S.S., Lokhande C.D., Joob O-S. (2009), *Electrodeposited porous and amorphous copper oxide film for application in supercapacitor*, Materials Chemistry and Physics 114, 6–9

[10] Dubal D.P., Dhawale D.S., Salunkhe R.R., Jamdade V.S., Lockhande C.D. (2010), *Fabrication of copper oxide multilayer nanosheets for supercapacitor application*, Journal of Alloys and Compounds 492, 26-30

[11] Eugénio S., Silva T. M., Carmezim M. J., Duarte R. G., Montemor M. F. (2013), *Electrodeposition and characterization of nickel–copper metallic foams for application as electrodes for supercapacitors*, Journal of Applied Electrochemistry

[12] Qu Q., Yang S., Feng X. (2011), *2-D sandwich-like sheets of iron oxide grown on graphene as high energy anode material for supercapacitors*, Advanced materials, Volume 23: 5574-5580

[13] Nikolic N. D., Popov K. I., Pavlovic L.J., Pavlovic M. G. (2007), *Phenomenology of a formation of a honeycomb-like structure during copper electrodeposition*, Journal of Solid State Electrochemistry, 11:667-675

[14] Matsushima H., Nohira T., Mogi I., Ito Y. (2004), *Effects of magnetic fields on iron electrodeposition*, Surface and Coating Technology 179, 245-251

[15] Conway B.E. (1999), *Electrochemical supercapacitors: Scientific fundamentals and technological applications*, Plenum Publishers

[16] Sinapi F., Deroubaix S., Pirlot C., Delhalle J., Mekhalif Z. (2004), *Electrochemical evaluation of the corrosion protection of bi-dimensional organic films self-assembled onto brass*, Electrochimica Acta 49, 2987–2996

[17] Ujimine K., Tsutsumi A. (2006), *Electrochemical characteristics of iron carbide as an active material in alkaline batteries*, Journal of Power Sources 160, 1431–1435

[18] Geana D., El Miligy A. A., Lorenz W. J. (1974), *Electrochemical behaviour of iron in Alkaline sulphate solutions*, Journal of Applied Electrochemistry 4, 337-345